Meteoritics & Planetary Science 39, Nr 9, 1475–1493 (2004)
Abstract available online at http://meteoritics.org

Analyses of the chondritic meteorite Orvinio (H6): Insight into the origins and evolution of shocked H chondrite material

Jennifer A. GRIER,[1] David A. KRING,[2] Timothy D. SWINDLE,[2*] Andrew S. RIVKIN,[3] Barbara A. COHEN,[4] and Daniel T. BRITT[5]

[1]Planetary Science Institute, Tucson, Arizona, USA
[2]University of Arizona, Lunar and Planetary Laboratory, Tucson, Arizona, USA
[3]Massachusetts Institute of Technology, Cambridge, Massachussets, USA
[4]University of New Mexico, Albuquerque, New Mexico, USA
[5]University of Central Florida, Orlando, Florida, USA
[*]Corresponding author. E-mail: tswindle@u.arizona.edu

(Received 30 July 2003; revision accepted 16 June 2004)

Abstract–We have studied the petrography, reflectance spectra, and Ar-Ar systematics of the Orivinio meteorite. Orvinio is an H chondrite not an L chondrite as sometimes reported. The material in the meteorite was involved in several impact events. One impact event produced large swaths of impact melt from H chondrite material surrounding relict clasts of chondrule-bearing material. Not only were portions of a bulk H chondrite planestesimal melted during the impact event, but shock redistribution of metal and sulfide phases in the meteorite dramatically altered its reflectance spectra. Both the melt and relict clasts are darker than unshocked H chondrite material, bearing spectral similarities to some C-class asteroids. Such shock metamorphism, which lowers the albedo of an object without increasing its spectral slope, may partially explain some of the variation among S-class asteroids and some of the trends seen on asteroid 433 Eros. Noble gases record the evidence of at least two, and perhaps three, impact events in the meteorite and its predecessor rocks. The most significant evidence is for an event that occurred 600 Ma ago or less, perhaps ~325 Ma ago or less. There is also a signature of 4.2 Ga in the Ar-Ar systematics, which could either reflect complete degassing of the rock at that time or partial degassing of even the most retentive sites in the more recent event.

INTRODUCTION

Impact cratering, and its end member, catastrophic disruption, is the primary process affecting asteroids. An effective study of the impact history of an asteroid requires that adequate amounts of impact melted (or sufficiently heated) material be delivered to Earth in meteorites so that the timing and extent of the impacts can be constrained. However, less than one percent of ordinary chondrite material in collections consists of impact melt (Scott et al. 1989). The lack of impact melted material available from chondrites has allowed important and fundamental issues in the evolutionary history of chondrite parent bodies to go unresolved, as well as the effects of impacts on the properties of asteroids (Kring et al. 1996).

L chondrites record a number of dominant impact events. Uranium/thorium-helium, K-Ar, and $^{40}Ar/^{39}Ar$ all indicate a major event affecting L chondrite material at ~500 Ma (Schmitz et al. 2003; Bogard 1995; Haack et al. 1996; Heymann 1967). Other clusters of ages have also been suggested at 40, 350, 880, and 2500 Ma (Alexeev 1995, 1998; Kring et al. 1996; Bogard et al. 1976).

The distribution of impact ages for H chondrites is quite different. H chondrites do not record any obvious specific thermal impact events in the last 3 Ga using $^{40}Ar/^{39}Ar$ methodology (see Table 1 [Bogard 1995; Grier et al. 1996; Kring et al. 1996]). They do record a broad peak in U, Th-He ages at 3–4 Ga (Wasson and Wang 1991) and a cosmic ray exposure (CRE) age peak at ~7–8 Ma (Graf and Marti 1995), and an analysis of ^{3}He and ^{4}He suggests the possibility of local heating and degassing about 200 Ma ago (Alexeev 1998). The large difference between the Ar-Ar age distributions of H and L chondrites may be the result of the different collisional evolution for the L and H chondrite parent bodies, a smaller fraction of H chondrites being highly shocked, or a statistical artifact due to fewer H chondrites than L chondrites being analyzed with argon age dating (Bogard 1995).

Orvinio is a classic impact melt-bearing H chondrite

Table 1. Listing of H chondrite meteorites for which $^{40}Ar/^{39}Ar$ degassing ages have been determined (after Bogard 1995). Also listed for each meteorite, where available, are U, Th-He ages and CRE ages.[a]

Meteorite	Class	D	Ar age Degassing Ma	Low	High	Ref	U,Th He Ma	CRE Ma
Orvinio	H6/S3	CL	–	325–600	3750	1	50	7.4
Orvinio	H6/S3	M	4200	900	4450	1	–	–
Orvinio	H6/S3	WR		800	1900	2	–	–
Charsonville	H6	–	270 ± 30	–	3000	2	550	66.1
Clovis #2	H6	–	<40	–	–	2	–	–
Dar al Gani 896	[b]	–	3704 ± 35	–	–	3	–	–
Dimitt	H4/S3	–	900	–	4000	2	–	6
Jilin	H5/S3	–	500 (3950)	<0.4	4300	2	1250	2.6
Kimble County	H6	–	600 ± 40	–	1100	2	805	9.7
Monroe	H4	–	1100	–	3500	2	1210	12.8
Monahans	H5	LCL	4533	–	–	4	–	6
Monahans	H5	DCL	–	–	4500	4	–	13–18
Monahans	H5	H	–	–	4330	4	–	–
Plainview	H5/S3	CL	3630 ± 70	–	3660	2	3410	6
Portales Valley		–	4486	–	–	5	–	–
Sweetwater	H5	–	290	–	2800	2	–	5
Ourique	H4	CL	4450 ± 20	–	–	6	–	–
Tulia	H	–	460 ± 20	–	–	2	1070	4.6
Ucera	H5	–	40	–	3200	2	–	16.2
Rose City	H6/S6	WR	–	380	2300	2	260	38.9
Rose City	H5/S6	M	3620 ± 10	700–200	3620	7	–	–
Travis County	H5/S4	–	830 ± 30	330	–	7	–	–
Yanzhuang	H6/S6	HR	130 ± 40	–	3000	7	–	3
Yanzhuang	H6/S6	MF	4090 ± 40	200	4500	7	–	–

[a]The first argon degassing age is that of a mid-range or plateau if such exists. The low and high are the low and high points of the profile, where available. "D" is the description of the sample used to obtain the argon age, where available: WR = whole rock, M = melt, MF = melt fraction, CL = clast, LCL = light clast, DCL = dark clast, H = halite and HR = host rock. Shock classifications from Stöffler et al. (1991); U, Th-He ages from Wasson and Wang (1991); CRE ages from Graf and Marti (1995), except for Monahans (Bogard et al. 2001) and Orvinio (data from Schultz and Kruse [1989], calculated in the manner of Eugster [1988]). Ar-Ar references are: 1 = this study; 2 = sources as listed in Bogard 1995; 3 = Folco et al. 2004; 4 = Bogard et al. 2001; 5 = Bogard and Garrison 1999; 6 = Kring et al. 2000; 7 = Kunz et al. 1997. Certain meteorites appear more than once on the list because different fractions of the meteorite have been dated by the argon method. The symbol "–" is used to cover items that were either not available or not applicable.

[b]Achondrite, interpreted as melted H chondrite.

meteorite consisting of unmelted clasts in a matrix of melt. Several stones appear to have fallen in 1872 near Rieti in Lazio, Italy after reports of a fireball and the sounds of detonations (Grady 2000; Salpeter 1957; Salvatori et al. 1986). Six of these fragments were recovered with a total mass of 3.4 kg, with the largest piece being 1.2 kg. These are now referred to as the Orvinio meteorite (Grady 2000). As a chondrite, Orvinio's history must include accretion, one or more impacts that caused degassing, and one or more disruptive impacts, the last of which sent it on its way to Earth. Therefore, we have examined this important melt-bearing meteorite to reinterpret its thermal history in the context of an H chondrite (Table 1) in the hopes of illuminating more of the impact history of the H chondrite asteroid parent body. In addition to both macroscopic and electron microscopic examination, we have determined reflectance spectra on subsamples of the meteorite (to elucidate how these impacts would affect the appearance of the parent body) and performed Ar-Ar analyses (to determine the timing of some of these events).

The major differences in mineralogy, reflectance spectra, and the Ar-Ar systematics of the various parts of the meteorite are manifestations of the same shock event. However, as we will see, the different histories of adjacent parts of the meteorite during and shortly after the shock lead to distinct differences in the way the shock is recorded.

EXPERIMENTAL PROCEDURES

Electron Microscopy

Major and minor element analyses (Table 2) were made with a Cameca SX-50 electron microprobe using wavelength dispersive techniques and an accelerating voltage of 15 kV. Analyses of most of the phases in the rock were run with a beam current of 20 nA and a beam diameter of ~1 μm. To avoid volatilizing alkali elements during the analyses of feldspathic materials, we analyzed these phases with a reduced beam current of 10 nA and a broader beam diameter

Table 2. Fa and Fs analyses of Orvinio. Orvinio is within the H chondrite range.[a]

Ref	Lithology	%Fa in olivine	%Fs in pyroxene
1	Clast 1	19.0	16.3
	Clast 2, phase A	18.9	
	Clast 2, phase B	19.1	
	Melt		14.0
2	Chondritic	18.6	16.5
	Melt	17.7	15.9
	Clasts	18.5	16.0
3	L chondrite	~23–26	~17–22
	H chondrite	~16–20	~14–17

[a]Sources are: 1 = this study and Kring et al. 1996; 2 = Scott et al. 1986; and 3 = sources as listed in Sears and Dodd (1988).

of 10 μm. The feldspars were typical for an H chondrite, and so are not discussed further. Well-characterized standards were used to calibrate the instrument and are described with additional details of our electron microprobe procedures in Kring et al. (1996).

Noble Gas Mass Spectrometry: ^{40}Ar-^{39}Ar Analyses

We analyzed argon in six samples from Orvinio: three clast samples (OCA1, OCA2, and OCA3) and three melt samples (OMA5, OMA6, and OMA7). The samples were hand picked from a crushed slice of the meteorite facing the portion used for thin section. These samples were irradiated at the University of Michigan along with terrestrial samples for 10 hr in position L-67 of the Ford Reactor. The samples were analyzed in a VG5400 noble gas mass spectrometer (equipped with ion counting) at the Lunar and Planetary Laboratory, University of Arizona. The gases were extracted with a resistance-heated, double-vacuum Ta furnace and purified by exposure to SAES getters in an all-metal extraction line. A J-factor (reflecting the efficiency of conversion of K into ^{39}Ar in the reactor) of (1.353 ± .0175) × 10^{-3} was determined from seven samples of the MMhb-1 hornblende monitor (519.4 ± 2.5 Ma [McDougall and Harrison 1999]). The neutron flux variation was characterized by sandwiching samples between these monitors.

The samples were processed in three separate runs on the mass spectrometer. The first run (samples OCA1, OMA5, and OMA6) was conducted within five months of irradiation. A small but detectable level of ^{37}Ar remained for two of these samples (OCA1 and OMA5), so K/Ca ratios could be determined, and changes in this ratio could be used to identify changes in the mineral(s) degassing. The second run (OCA2 and OCA3) and third run (OMA7) were conducted several months later, so no appreciable reactor-produced ^{37}Ar remained. However, K/Ca ratios for these samples were estimated by proxy by looking at the ^{39}Ar/^{38}Ar ratios, and where they could be compared, the ^{39}Ar/^{38}Ar and ^{39}Ar/^{37}Ar plots exhibited similar behavior. Although we would expect some ^{38}Ar to be produced in our irradiation by neutron capture on ^{37}Cl (Garrison et al. 2000), ^{39}Ar/^{38}Ar and ^{39}Ar/^{37}Ar correlate reasonably well for OCA1, suggesting that this meteorite does not contain a large amount of Cl. Sensitivity for the first two runs was 2.42 × 10^{-14} cm^{3}STP/cps, and that for the last run was 3.14 × 10^{-15} cm^{3}STP/cps. Sensitivities were determined by measurements of aliquots of air (measured ^{40}Ar/^{36}Ar = 293 ± 3). All errors are 1σ, and correlated errors are taken into account.

Blanks were temperature dependent, with ^{40}Ar amounts as follows: run 1: <5 × 10^{-10} cm^{3}STP below 1100 °C and <1.5 × 10^{-9} cm^{3}STP up to 1400 °C; run 2: <3 × 10^{-10} cm^{3}STP below 1200 °C and <5 × 10^{-10} cm^{3}STP up to 1500 °C; and run 3: <5 × 10^{-11} cm^{3}STP below 1200 °C and <2 × 10^{-10} cm^{3}STP up to 1400 °C. The data shown in the Tables A1–A6, used for the generation of argon release profiles, Arrhenius (diffusion) plots, and for the calculation of apparent ages, have been corrected for blanks, interfering reactions, and decay of ^{39}Ar. Corrections for ^{39}Ar produced by reactions on Ca were insignificant in the cases where we had ^{37}Ar data to use for the correction and so were not applied to the other samples. The error shown in Tables A1–A6 for the apparent ages is the total error, including the uncertainty in the J factor and the age of the monitor. Full sets of K/Ca, three-isotope, and Arrhenius plots are available electronically from the correspondence author.

Reflectance Spectroscopy and Point Count Analyses of Opaque Material

Small samples of the melt and clast phases were hand-selected from a crushed portion of Orvinio. These samples were taken from areas immediately adjacent to the area sampled by thin section so that the reflectance spectra could be correlated with the distribution of opaque phases (below). Two phases of clast material were recognized, one much darker than the other. Therefore, we refer to the two types of clast material as "light" and "dark," although these are relative terms. Both clast phases in this shock-darkened meteorite are dark compared to the clastic material of chondritic breccias. The dark phase constituted only a very small fraction of the available clast material and could not be physically separated from the light clast material. The reflectance spectrum for "clast," therefore, is a mixture of the two clast phases with the mass dominated by the light clast phase (only OCA3 of the noble gas samples contained any dark clast material, and it was dominated by light clast). The samples of both clast and melt were ground to a size of <125 μm. The Reflectance Experiment Laboratory (RELAB) facility at Brown University was then used to obtain bi-directional reflectance spectra from 0.3–2.6 μm (Pieters 1983). Further description of this technique can be found in Britt (1991).

Point counts were made of the distribution and size of opaque phases in the clast and melt material of Orvinio. For the light clast, dark clast, and melt areas, areas of 10.4, >5.5, and 7 mm^2, respectively, were covered with 1072, 1487, and 1824 points, with spacing of 47, 30.5, and 30.5 μm. When a point was metal or sulfide, the size of the particle was measured.

RESULTS

Description of Sample

Our specimen of the Orvinio meteorite was obtained from the Vatican Observatory (Specola Vaticana) Meteorite Collection (courtesy of Dr. Guy Consolmagno, see listing [Salvatori et al. 1986]). Originally, this meteorite was listed in the *Catalogue of meteorites,* Specola Vaticana, as a bronzite-chondrite (i.e., a high iron content or H chondrite) in 1957 (Salpeter 1957). Subsequent to this, an extensive survey of the olivine compositions of ~800 meteorites, as determined by X-ray diffraction measurements, was conducted by Mason (1963). In this survey, Orvinio is listed as Fa_{23}, where olivine-hypersthene chondrites (L) were defined as $Fa_{22–31}$, and olivine-bronzite chondrites (H) were defined as $Fa_{15–21}$. Scott et al. (1986) re-examined Orvinio and six other chondrites containing impact melt and showed that Fa and CaO in olivine and Fs and Wo in pyroxene for Orvinio were all consistent with an H classification for Orvinio, not the L classification previously reported by Mason (1963). The results of Scott et al. (1986), however, appeared only in abstract form, and most researchers conducting recent studies on chondrites appear to have missed it (i.e., Graham et al. 1985; Salvatori 1986; Wasson and Wang 1991; Graf and Marti 1995; Bogard 1995). Our analyses, indeed, confirm the H chondrite classification of Orvinio as indicated in Scott et al. (1986) (see also Grady 2000). Our measurements of Orvinio clasts indicate a %Fa in olivine of 19.0 ± 0.5; well inside the H chondrite range (See Table 2), and pyroxene compositions are $Wo_2En_{82}Fs_{16}$, typical of H chondrite material.

Orvinio is composed of unmelted chondrule-bearing clasts in a matrix of impact melt that appears to have been produced from a target of the same chondritic material. The texture of the clasts indicates that, before the material in Orvinio was shock-metamorphosed, it was thermally metamorphosed to an H6 state (Scott et al. 1986; Stöffler et al. 1991).

Like the Cat Mountain impact melt breccia (Kring et al. 1996), Orvinio is a relatively dark ordinary chondrite. Unmelted relic clasts are medium dark gray (N4; Rock-Color Chart Committee 1991) on a rough surface and dark gray (N3) on a sawn surface. The melt has a slightly lighter color than the clasts in a sawn surface, between medium dark gray (N4) and dark gray (N3). Metal and sulfide are heterogeneously distributed in the meteorite. These opaque phases are finest in a <1 mm-wide boundary layer of melt around the clasts in what appears to be a zone of melt that was quenched on cold clasts. Farther from the clasts, the metal and sulfide in the melt is coarser and shows flow alignment.

The clasts have a complex structure. The largest clast (at least 2.5 × 1.0 cm in size, but truncated by the edge of our specimen) has three distinct zones. The middle zone looks like relatively normal H chondrite material, with relic chondrules, although some chromite grains have been disrupted. A similar level of shock was seen in clastic material in Cat Mountain (Fig. 4b of Kring et al. 1996). This zone is bounded by two very dark zones of material that are characterized by very finely disseminated metal and sulfide particles. One of these zones is also crosscut with metal-sulfide veins.

The melt contains euhedral to subhedral olivine and pyroxene grains, typically 5 to 50 μm in diameter, with interstitial feldspathic mesostasis (Fig. 1). Texturally, the silicates are very similar to those in the melt phase of Cat Mountain (Fig. 5a of Kring et al. 1996). Metal and sulfide usually occur together. Many mixed metal-sulfide particles are comparable in size to the silicates, although they also exist as larger (mm-scale) elongated particles in which orbicular metal is embedded in sulfide. This texture is also found in the melt phase of Cat Mountain (Fig. 5c of Kring et al. 1996).

Distribution of Opaque Phases

The shock processes that affected Orvinio have redistributed the opaque phases in the melt and clast fractions. This redistribution may have affected the reflectance properties of the material as well as that of the meteorite's parent body. Britt and Pieters (1991) noted that the redistribution of opaque phases into ~1 μm-sized or nanophase particles dramatically darkens the reflectance spectra of meteorites. A point count analysis was made to assist in quantification of any spectral differences between "dark" meteorites and those that have not been heavily shocked. Like Cat Mountain (Kring et al. 1996), Orvinio offers an opportunity to compare the spectral effects of redistributed opaques in both the impact melt fraction and the clast material.

Figure 2a is a histogram of the point count and particle sizes for the light clast portion of Orvinio (the number of particles is smaller than the number of points at larger sizes, where multiple points fall on single particles). The distribution represents all sizes relatively equally, with a few large shock veins dominating the large particle size in the number of points. This lighter clast portion represents an area less affected by shock redistribution of opaques. The darker clast portion, illustrated in Fig. 2b, shows a strong redistribution of opaques to the smaller sizes. The

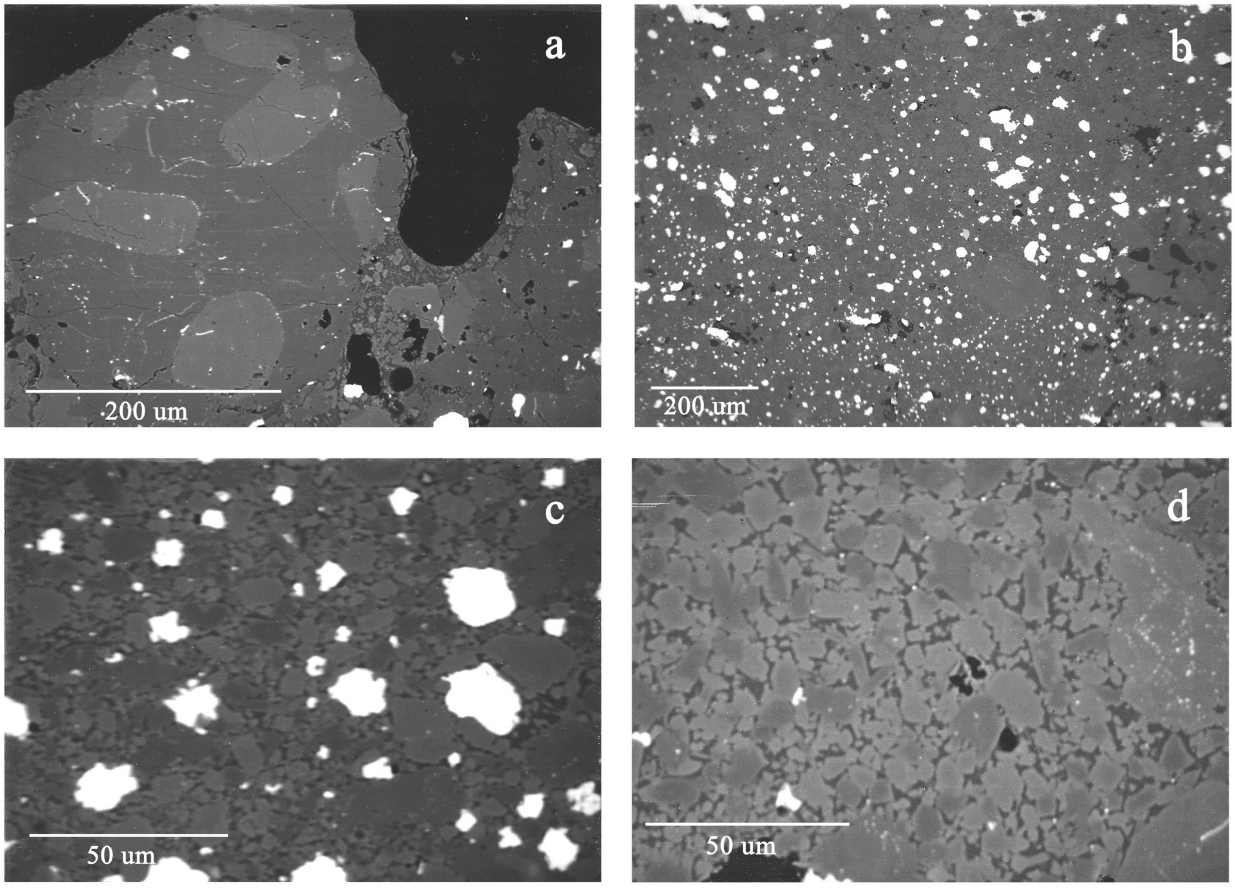

Fig. 1. Backscattered electron images of Orvinio: a) unshocked portion of the chondrite with a granular olivine-pyroxene chondrule (left) and adjacent matrix and the edge of an additional chondrule (right). The edge of the thin section is apparent, and the surrounding epoxy is dark. The scale bar is 200 μm long; b) shock-melted portion of the chondrite illustrating the relatively fine-grained mixing of silicate minerals with metal and sulfide particles. The scale bar is 200 μm long; c) a close-up view of a metal- and sulfide-rich portion of the impact melt. The scale bar is 50 μm long; d) a close-up view of a metal- and sulfide-poor portion of the impact melt. Silicate crystals are less than 50 μm in diameter and typically less than 10 μm in diameter. The scale bar is 50 μm long.

distribution is somewhat bimodal, but large patches of opaques dominate the point counts at larger sizes. The point count for the melt lithology is in Fig. 2c. As expected, the melt has few particles in the smaller sizes, much like the light clast portion. The spike in the number of particles at larger sizes may be due to the agglomeration of metal and sulfide particles. If the material remained molten long enough, this would allow the metals to form bigger droplets. Consistent with the observation of Britt and Pieters (1991), the dark clast portion was most affected by the redistribution of opaques.

The melt, dark clast, and light clast portions of the Orvinio meteorite have, respectively, 8.6%, 24.6%, and 15.1% of points identifiable as metal and sulfide. This suggests that, at least within the region represented by the thin section, metal and sulfide were locally redistributed from one area to another. However, the spectral differences are a result of the distribution of metal and sulfide among grain sizes not the total amount present.

Comparative Reflectance Spectra of Clast and Melt Fractions

Figure 3 shows the reflectance spectra of the Orvinio clast and melt phases. As mentioned previously, for the purposes of reflectance spectra, the clast portion is a mixture of both dark clast and light clast phases, with the light clast phase comprising the bulk of the material. The clast spectrum is darkened and subdued compared to the less shock-darkened melt material. The clast phase has a reflectance of 0.085 at 0.55 μm, which is typical of the 0.08–0.12 range of pristine shock-blackened ordinary chondrites (Britt and Pieters 1994). The melt phase, while somewhat less shock darkened, has a reflectance of 0.10 at 0.55 μm, also well within the typical range. The spectral band depth at 1.0 μm (which indicates the presence of pyroxene and some olivine) is quite different for the two phases. The 1.0 μm band of the clast phase is attenuated compared to the same band position in the melt phase. Both spectra also possess a very broad feature at about

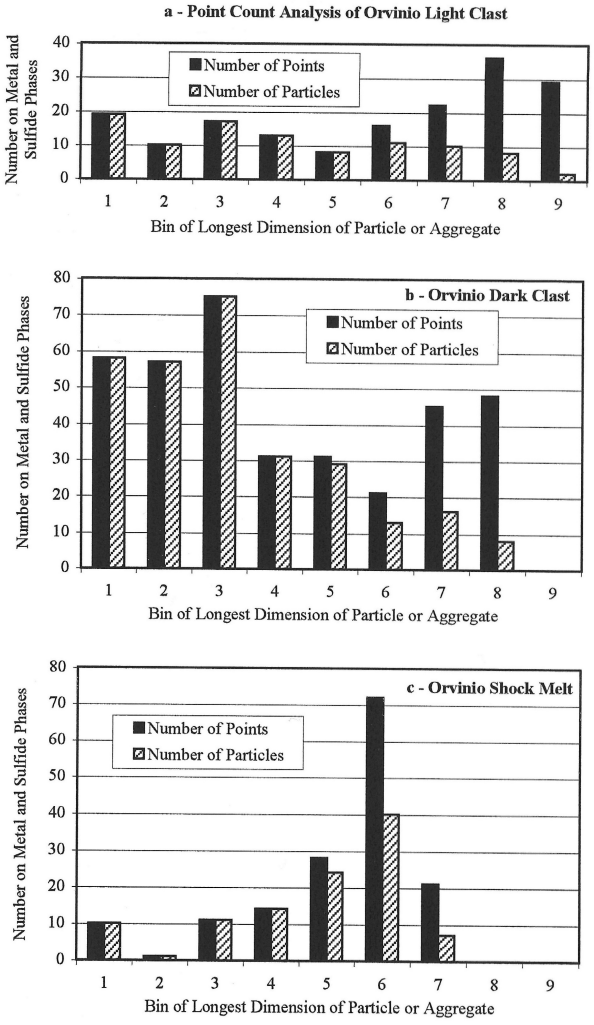

Fig. 2. Histograms of point count analyses and particle sizes of Orvinio metal and sulfide. The solid bars represent the number of points that fell on a particle of a particular size. The hatched bars represent the number of particles encountered and serve as a reminder that a large number of points on large particles does not mean a large number of large particles, since several points will fall on the largest grains. These data show the redistribution of opaques. The melt phase has a substantially larger number of opaque particles in the intermediate size range compared to the shock-darkened clast phase, which is dominated by particles in the 1 μm range (see text). Bin sizes from 1 to 9 for (a) and (c) are (in μm): <1, 1–3, 3–15, 15–30, 30–61, 61–152, 152–305, 305–1000, and >1000. For (b), bin sizes are <1.6, 1.6–4.7, 4.7–23.6, 23.6–47.2, 47.2–94.4, 94.4–236, 236–472, 472–1685, and >1685.

2 μm, indicative again of pyroxene. This feature is also subdued in the clast spectrum versus that of the melt.

These spectra indicate that, despite the fact that the light clast portion is by far the larger part of the sample, the spectral signature of the dark clast material dominates the overall spectrum of the clast phase. Otherwise, as indicated by the discussion on the opaque counts, we might expect the light clast to be quite bright and the light clast and melt to show much less of the subdued shock darkening of the dark clast phase in comparison.

Figure 4 shows the normalized Orvinio spectra compared to the "average" H5 and H6 chondrites, undarkened, from Gaffey (1976), with the data in the top figure normalized to equal 1 at 0.55 μm. The average spectra have deep, unattenuated features at 1 and 2 μm, and the slope in the UV is very steep compared to Orvinio. This illustrates a continuum of levels of shock darkening, from the average H6 (least attenuated bands), to Orvinio melt, to Orvinio clast with the most attenuated bands. The bottom panel shows the absolute reflectance of these samples, where the overall reduced reflectance of Orvinio relative to the average H5/H6 spectra is clearly illustrated.

^{40}Ar-^{39}Ar Chronology

Tables A1–A6 list the experimental argon data obtained from each of the six samples. The release spectra of apparent ^{40}Ar/^{39}Ar ages are shown in Fig. 5. The three clast samples have similar argon age spectra shapes and attain the same approximate ages in the higher temperature steps (Fig. 5a). But the three clast samples are not consistent in the low points they achieve (~325 Ma, ~570 Ma, and ~710 Ma), exhibiting various levels of degassing. The degassing patterns shown in Fig. 6 (after Trieloff et al. 1994) indicate that the main ^{39}Ar release for the clast samples occurred in two major degassing intervals with peaks at ~600 °C for the first interval and around 1100 °C for the second. A K/Ca plot for sample OCA1 (Fig. 5a) shows a bimodal nature, indicating that the sample may have been degassing separate mineral phases (or groups of mineral phases) with differing argon retentivities at the lower and higher temperatures. Plots of K/Ca for the other two clast samples (not shown) are similar, as expected.

Two of the melt samples (OMA5 and OMA6) have consistent low points achieved in the argon age spectra (~900 Ma) and in the "plateaus" reached in higher temperature steps (~4200–4300 Ma) (Fig. 5b). The third melt sample (OMA7), however, has a strongly curved saddle-shaped profile that bottoms out at an age of about 525 Ma and reaches its highest point at ~4100 Ma. The first two melt samples have similar degassing behavior, with the dominant fraction of the gas released in the high temperature steps (1250 °C–1400 °C), and a change in K/Ca. Their release plots indicate that the degassing was somewhat bimodal, like the clasts, with a suggestion of two separate degassing domains. However, the third melt sample shows a single, broad degassing interval from 400 °C to 800 °C. The Arrhenius plot for this sample (discussed below) is quite linear and does not indicate multiple degassing domains, nor does a K/Ca plot (not shown). The lower ages in the clast material, as compared to the melt fraction, indicate some measure of incomplete degassing of the melt material during a thermal event (Bogard et al. 1995).

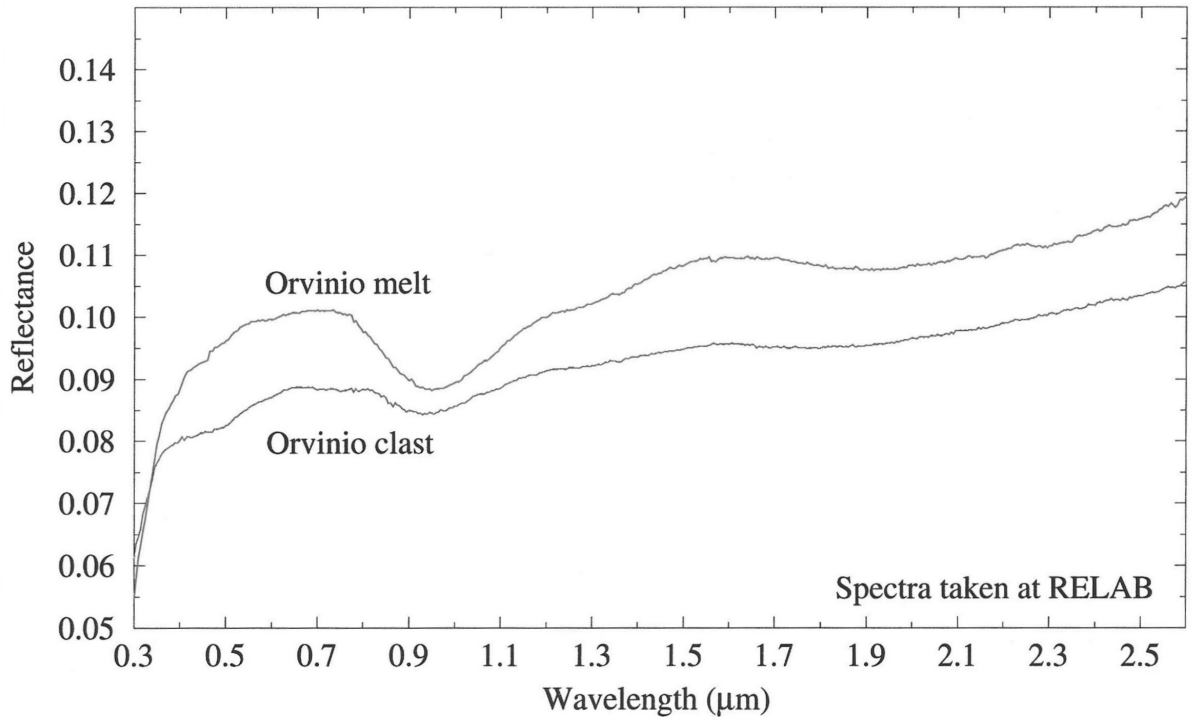

Fig. 3. Reflectance spectra of Orvinio melt and clast phases. The spectrum for the clast phases shows the shock darkening of the spectra and the dampening of the strength of the absorption features at ~0.9 and ~2.0 μm. The clast phase for Orvinio is a mixture of "light" and "dark" clast material, with the "light" material comprising the bulk of the analyzed sample.

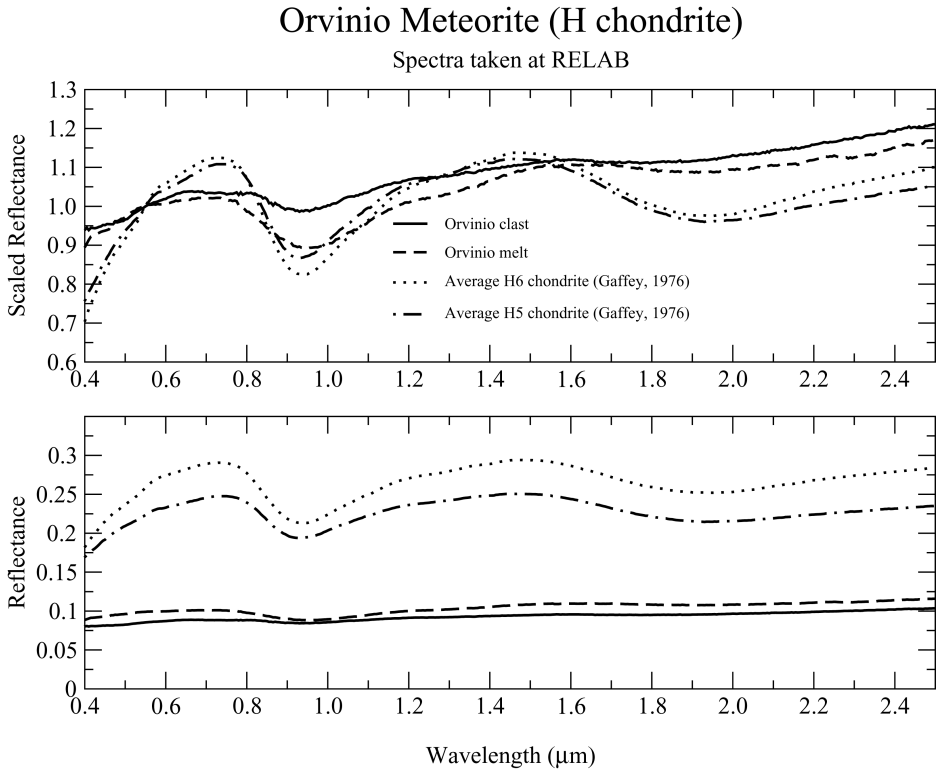

Fig. 4. Reflectance spectra of Orvinio melt and clast phases with average H5 and H6 chondrites (Gaffey 1976). Note the spectral effects shock darkening, including strongly reduced reflectance and strongly attenuated absorption features relative to the average H5/6 ordinary chondrite. The spectra are normalized to equal 1 at 0.55 μm in the top panel.

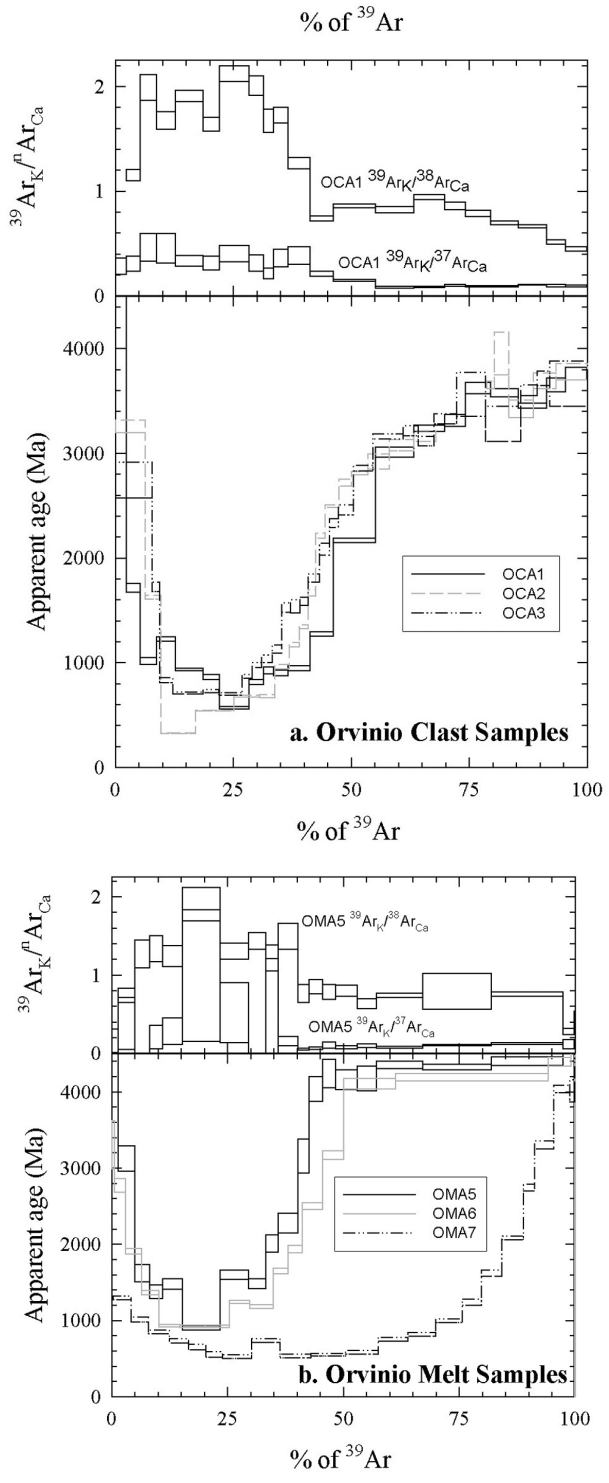

Fig. 5. Argon age profiles of the Orvinio clast and melt phases. The earliest fractions of the release, in some cases, show contamination by atmospheric argon. For clast sample OCA1 and melt sample OMA5, the two samples for which we had sufficient Ca-derived ^{37}Ar remaining to be above background, K/Ca ratios (actually, $^{39}Ar_K/^{37}Ar_{Ca}$) are also shown. We would expect the ratio to be higher in the lower-temperature steps, since potassium feldspar, a likely K carrier, has a lower retentivity and higher K/Ca than most other minerals present.

The strongly saddle-shaped argon release profile in OMA7 is another possible indication of incomplete degassing. Lanphere and Dalrymple (1976) suggested that profiles of this nature indicate that the sample was not completely degassed during shock metamorphism, leaving an excess of ^{40}Ar behind in the rock. Whole rock argon studies of Orvinio (Bogard and Hirsch 1980) also indicated incomplete degassing. Another factor that can contributes to the saddle shape is terrestrial air incorporated into the sample, which would produce artificially high apparent ages at the low temperatures at which it would preferentially degas. There is no objective way to determine how much terrestrial Ar is incorporated in any extraction, because ^{36}Ar, the isotope used as a tracer for air in terrestrial work, can also come from either trapped ("planetary") or spallogenic gas in a meteorite. However, trapped and spallogenic gas are usually released at higher temperatures, so if we arbitrarily assume that all ^{36}Ar in all steps before the minimum in apparent age is the result of air, we can subtract the amount of ^{40}Ar that would accompany the ^{36}Ar (if we correct for spallation, the high-temperature extractions have little residual ^{36}Ar). Except for the first step or two, for OCA1, OCA2, OCA3, and OMA7, all the steps before the apparent minimum age give ages of 320 to 630 Ma. For the less-degassed OMA5 and OMA6, the apparent ages are still >740 Ma. Although there may be a significant amount of incorporated air, this treatment still will not generate plateaus at the lower temperatures.

We also considered three-isotope plots in an attempt to search for evidence of "excess" ^{40}Ar that could cause the saddle-shaped profiles. If we corrected for spallation, plots of ^{39}Ar/^{40}Ar versus ^{36}Ar/^{40}Ar (not shown) showed no signs of any linear array suggestive of a single trapped pseudo-component containing "excess" ^{40}Ar in any sample.

To glean more information, we examined the Arrhenius plots (e.g., Fig. 7) for each sample. There appear to be two principal degassing domains in most samples (Fig. 6), and since a plot such as Fig. 7 includes gas released from both domains, the assumptions going into the calculations are not strictly valid. However, since there appears to be little overlap in the release of gas from the two domains in most samples, we can split the data for each sample (except for OMA7, with no high-temperature domain). Then, we can generate Arrhenius plots and calculate diffusion parameters for each domain (Fig. 7, solid points; after Bogard and Hirsch 1980). From the slopes of these plots, we calculate activation energies (E) of 15 to 34 kcal/mol. Even for feldspars, which have some of the lowest Ar retentivities of measured minerals, activation energies are usually 35–50 kcal/mol (Foland 1974), but Orvinio's may have been affected by shock. For the high temperature domains, we calculate E of about 45 for OCA1 and OCA2, ~65 for OCA3 and OMA6, and 235 for OMA5. The first four of these are quite reasonable (cf., McDougall and Harrison 1999, section 5.7). For OMA5, the result suggests that the assumptions of the

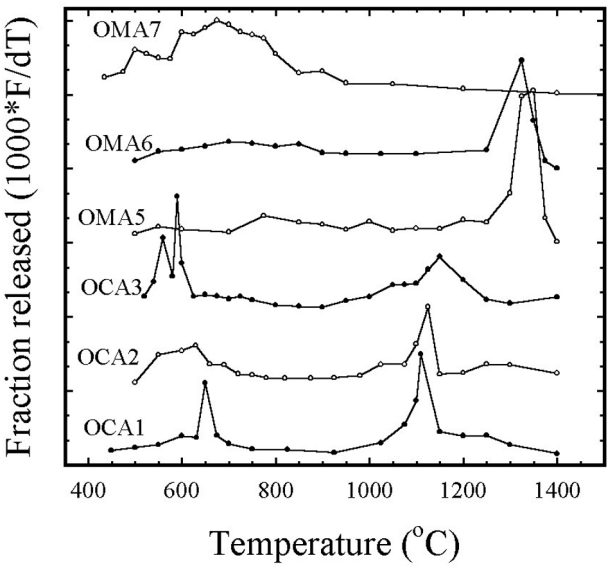

Fig. 6. Argon release patterns as a function of temperature for the Orvinio clast and melt phases, given as the fraction of the total ^{39}Ar in a sample released per degree of heating. For ease of comparison, the release patterns are offset by 3.0.

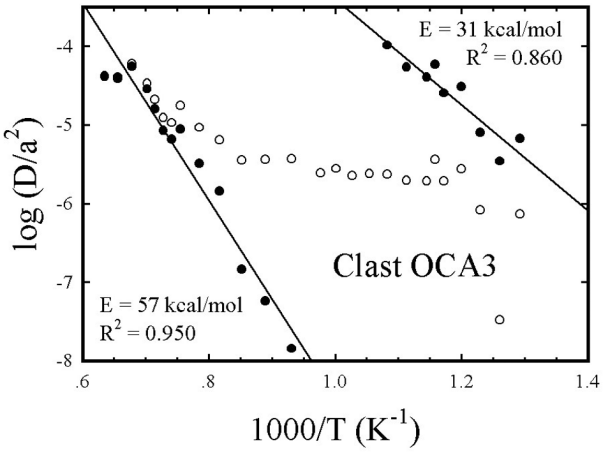

Fig. 7. Arrhenius plots for the Orvinio clast OCA3, which has a prototypical bimodal release pattern (see Fig. 6). Open points represent calculations assuming all gas comes from a single diffusion domain. Solid points represent re-calculations assuming there are two degassing domains and taking the data from 500 to 675 °C as the low temperature domain and 800 to 1400 °C as the high temperature domain and treating them independently.

calculations may have broken down—for example, the sharp release spike (Fig. 6) that is responsible for the high apparent E could be the result of sudden onset of melting, although we do not understand the reason that none of the other samples showed such behavior.

Coupled with the frequency factor (also calculated from Arrhenius plots) and the cooling rate (15–100 K/day; Smith and Goldstein 1977), we can calculate closure temperatures. Despite the large variation in calculated diffusion parameters and the order-of-magnitude uncertainty in cooling rate, the closure temperatures are all 255–590 °C for the low temperature domains and 760–1470 °C for the high temperature domains. There is a difference of 430–840 °C between the two domains in any given sample. For both the high and low temperature domains, the melt samples all yield higher closure temperatures than the clast samples, with one exception (OMA5 versus OCA3, using low cooling rates). This is consistent with the apparent ages seen—the clasts, with lower calculated closure temperatures, reach lower apparent age minima and lower apparent age maxima. For a polymineralic set of samples such as ours, the diffusion effects of several minerals, which themselves may contain several diffusion stages, cannot be separated out, so our treatment as a two-component system is still an oversimplification, but the results do support diffusion-controlled degassing in the recent impact event.

The apparent ages of 4.2–4.3 Ga may record the timing of an earlier impact event. The only remaining suggestion of this is the plateaus in the high retentivity sites in the Ar spectra for two of the melt samples (Fig. 5b). It is also possible that these are not true plateaus and merely represent either less degassing or more incorporation of parentless ^{40}Ar during a more recent event.

Meanwhile, the sites of lower retentivity in the melt and clast fractions only offer an upper limit to the age of the impact that partially degassed them (Jessberger et al. 1976). This event occurred ~600 Ma ago or less, perhaps ~325 Ma ago or less. A total of six steps (in various samples) have apparent ages of 500–600 Ma (and another eight have apparent ages of 600–740 Ma), so 500–600 Ma might represent the actual age of an event. An age of 500–600 Ma also corresponds to the lowest points achieved in a near plateau in the OMA7 sample, although we have noted this sample's strongly disturbed spectrum. However, there is a single younger step, 324.1 ± 5.5 Ma, in the apparent age spectrum of OCA2. We see no reason to reject this datum, so ~325 Ma may be a better upper limit to the time of this event. Regardless of the validity of that single datum, we can say with confidence that the event occurred no earlier than ~600 Ma ago. This event, which is presumably the event that created the melt, left excess Ar trapped in the more retentive melt samples to varying degrees, and the less retentive clast samples remained "open" to Ar longer. A few days or weeks after the event, the local temperatures dropped below ~250 °C, and all of the sites finally closed, leaving signatures of various levels of degassing in the clast phases of the meteorite.

DISCUSSION

Collisional and Thermal Impact History of the Orvinio Meteorite

Degassing and successful resetting of Ar depends on mineral retentivities, post-impact temperatures, and cooling

rates of the impact melt breccias, as noted from studies of the L chondrites Peace River, Chico, and Cat Mountain (Bogard et al. 1995; Kring et al. 1996; McConville et al. 1988). Two cooling rates are generally discussed with respect to impact melts. The first cooling rate is that associated with the rapid quenching of melt as it comes into contact with cold clastic material and achieves thermal equilibrium with the clastic material. This cooling phase, which is extremely rapid, determines the mineralogic and, hence, spectral properties, but little or no degassing occurs because of the short time involved. The second phase of cooling occurs more slowly, as the entire sample of clast and melt slowly dissipate heat into their surroundings and into space. This is the cooling rate associated with the argon degassing of the meteorite sample and with the diffusion within metal grains (used to calculate the quoted cooling rate). In Orvinio, the diffusion properties of the melt made it more difficult to degas in the second phase, so it is less degassed than the clast despite having experienced higher instantaneous temperatures. Peace River appears to be an end member case of rapid cooling, its glassy (quickly cooled) melt containing a large amount of excess Ar and the clasts showing younger ages near 430 Ma. Orvinio also cooled relatively quickly (~5000 to 40,000 K/yr; Smith and Goldstein 1977) and is less completely degassed than Chico, which cooled more slowly (0.01 to 1 K/yr; Bogard et al. 1995). The degassing history of these meteorites is in contrast to the L chondrite Cat Mountain. Cat Mountain appears to be more thoroughly degassed, with a cooling rate (~0.1 K/yr) similar to or less than that of Chico. Unlike Peace River or Orvinio, Cat Mountain's melt and clast phases all appear to be consistent with an 880 Ma age (Kring et al. 1996).

In spite of the complexities of cooling rates and argon retentivities, our study of both clast and melt samples in Orvinio allow constraints to be placed on the history of the meteorite. We can infer from the presence of chondrules in the meteorite that the Orvinio H chondrite parent body accreted ~4550 Ma (Kring et al. 1996). There is some evidence that the body experienced a large impact at about 4200 Ma that reset argon in the most highly retentive sites. Subsequent to this, ≤600 Ma ago (perhaps ≤325 Ma ago), the material experienced a thermal impact event that partially degassed some argon from all but the most retentive sites. The rapid cooling rate of the meteorite suggests that it need not have been buried more than about a meter deep in the parent body (Smith and Goldstein 1977). Sometime between this impact and 7.5 Ma, there was probably another impact, which ejected material from the asteroid parent body. As the material evolved into an Earth-crossing orbit, a final impact or set of impacts occurred that reduced the fragment to a meter-sized object about 7.5 Ma, as evidenced by its CRE age. Eventually, the object broke apart as it entered Earth's atmosphere in 1872, and the pieces became the meteorite Orvinio.

Spectral Effects and Implications for Meteorite-Asteroid Correlations

Since the reflectance spectrum of the clast phases is dominated by the dark clast portion, even though the light clast portion comprises the bulk of the sample, it appears that a relatively small amount (<20%) of shock-darkened material in a meteorite will change its reflectance spectrum. This is consistent with the work of Clark (1983), who noted that small amounts of low albedo material dominate the reflectance spectra of materials created from multiple phases with differing albedos. This has obvious implications for comparison of asteroid and meteorite spectra when searching for the parent asteroids of chondrites with a shock-darkened component.

Lunar soils show evidence of spectral changes with increasing exposure to solar wind and micrometeorite impacts, changes that tend to be grouped under the term "space weathering." Lunar space weathering has been attributed to the reduction of FeO in soils to Fe, followed by vapor deposition of the Fe on grain boundaries (Noble et al. 2001; Pieters et al. 2000). This process tends to decrease albedos and band contrast and increase spectral slopes.

Data from the NEAR Shoemaker Eros encounter show that that body has both bright and dark areas (Clark et al. 2002), with the bright areas associated with fresher material and darker ones associated with "mature," background regions. Eros also appears to have an ordinary chondrite composition, except for a depletion in sulfur (Nittler et al. 2001). Therefore, it is reasonable to compare observations of Eros' surface to Orvinio, a sample of an ordinary-chondritic asteroid. In Fig. 8, we compare the Orvinio spectra to bright and dark areas on Eros. Both the clast and melt portions of Orvinio are much darker than the dark region on Eros shown. While brighter and darker areas exist on Eros, the spectral slopes do not appear to be different between these areas. It is possible that shock darkening like that seen in Orvinio is at least partially responsible for the dark areas, since it does not involve a change in spectral slope.

Although an asteroid with a surface that is entirely or largely composed of Orvinio-clast or -melt material is not expected, it is instructive to imagine how such a body would be classified based on its spectrum. In the Bus and Binzel (Bus and Binzel 2002) taxonomy, which uses 0.45–0.92 μm data, the Orvinio clast material would be unambiguously grouped with the C-class asteroids, while the melt material is difficult to classify, falling closest to the Sq and C taxa (Binzel, personal communication). The C-class asteroids are thought to be analogous to the carbonaceous chondrites (Gaffey et al. 1989), while the Sq class, in the Bus and Binzel taxonomy, are qualitatively similar to ordinary chondrite meteorites. The albedos of the Orvinio samples are also comparable to C-class asteroids, and it is likely that, if Orvinio were an NEA, it would be included among the C-class asteroids without

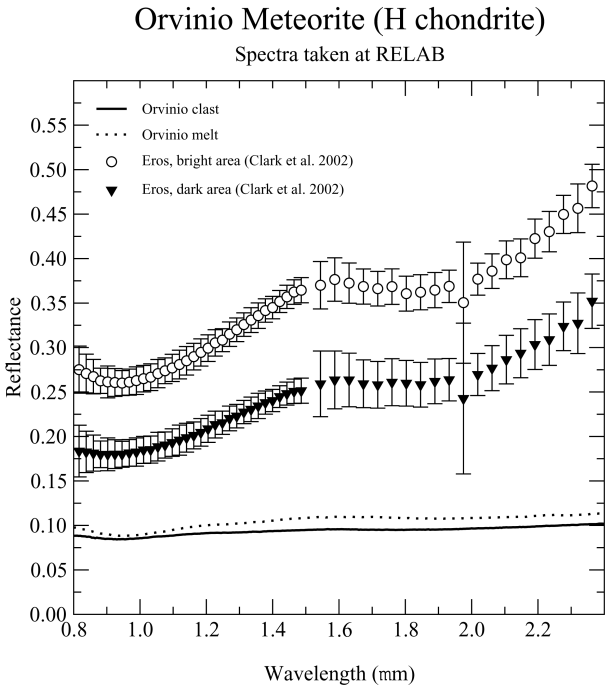

Fig. 8. Spectra of Orvinio melt and clast compared with spectra of both bright and dark areas of asteroid 433 Eros measured by NEAR Shoemaker (Clark et al. 2002).

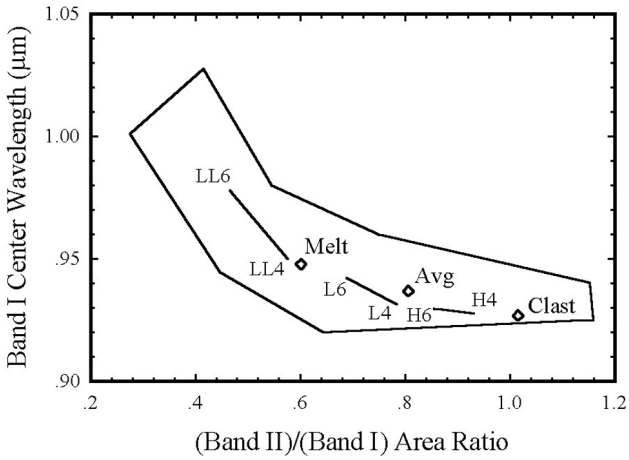

Fig. 9. Location of the band I center (near 1 μm) plotted against the ratio of areas of band II (near 2 μm) to band I for the different metamorphic and chemical classes of ordinary chondrites. Neither the Orvinio clast nor the Orvinio melt fall in the region with the most unshocked H6 chondrites. Figure adapted from Gaffey and Gilbert (1998).

further thought. We note again that bodies several km in size are not expected to be dominated with Orvinio-clast or -melt material, but shock darkening may account for some of the variation in S-class asteroids that is seen.

Gaffey et al. (1993) showed that when the band I center (near 1 μm) was plotted versus band area ratio (ratio of areas of the 1 μm and 2 μm bands), the ordinary chondrite meteorites clustered in a specific part of the space. Gaffey and Gilbert (1998) refined this diagram to allow for specific types of OC meteorites to be distinguished. When placed on such a diagram, the Orvinio samples do not act as might be expected (Fig. 9). Although the samples are H6, and an average of the clast spectrum and the melt spectrum would fall near the area expected for an H6, the spectrum of the clast would lead one to classify it as H4, while the melt is in the LL region, near LL4. When applying this to interpretation of asteroid spectra, it is clear that differing amounts of melt and clast on asteroid surfaces may skew the results. Even relatively small amounts of melt may pull the spectrum out of the H chondrite region, particularly if it is in an intimate mixture with unshocked material, which would allow it to exert an influence greater than its volume fraction.

Implications for Impact Processing of H chondrites

Table 1 lists all the H chondrite meteorites for which $^{40}Ar/^{39}Ar$ ages have been obtained. While no obvious, dominant events are seen like the ~500 Ma event in L chondrites, there is evidence to suggest the timing of some particular impacts affecting H chondrites. First, a summary of K-Ar ages of H chondrites (Alexeev 1998) shows a broad peak at ~4.3 Ga (their Fig. 1), perhaps either an impact event or partial minor degassing of 4.55 Ga material in one or more later events; either could explain the ~4.2 Ga age seen in Orvinio, although the apparent plateau at higher temperatures in OCA5 is more consistent with complete resettting in an early impact. Charsonville, Rose City, Sweetwater, and Travis County all have indications of degassing ages (either plateaus or upper limits) of 270 to 380 Ma, similar to Orvinio's possible degassing age of ~325, so perhaps, some H chondrite material experienced an impact at ~300 Ma (in this scenario, Orvinio's and other slightly higher upper limits would represent incomplete degassing). However, many scenarios for the impact history in the last 1 Ga can be constructed from the data in Table 1, involving various degrees of resetting in events at various times, and data on more H chondrites is clearly needed to sort it all out.

The history of the H chondrite parent body or bodies over the last 1 Ga cannot have been too simple, though. For example, Orvinio and Rose City both have some evidence for an impact 380 Ma ago or less but have CRE ages of 7.4 and 38.9 Ma, respectively. If they were part of the same event ~300 Ma ago, this requires at least two different impacts to reduce them to the objects that finally collided with Earth.

CONCLUSIONS

Orvinio is an important H chondrite impact melt breccia meteorite. Given the paucity of impact melt material found in ordinary chondrites, studies of Orvinio offer significant opportunities for understanding the nature and genesis of shock-darkened meteoritic material and the impact histories

of the asteroid parent bodies from which this material comes. Orvinio fell to Earth in 1872 and has been alternately termed both an L and H chondrite in the recent scientific literature. We have confirmed the results of Scott et al. (1986), which unequivocally place this meteorite in the H class.

Studies of this and other similar meteorites have made clear that the $^{40}Ar/^{39}Ar$ system is not completely reset in all events affecting impact melt breccias. This affirms the need to be careful when trying to determine the timing of thermal events that have affected these rocks (Bogard and Hirsch 1980). Shocked rock, in particular, seems to possess a wide range of behaviors with regard to Ar degassing (Deutsch and Scharer 1994). In spite of these difficulties, meaningful information concerning the impact histories of shocked chondrites and their parent bodies can be extracted. Continued research into the degassing behavior of individual minerals common to meteorites may allow for their complex thermal histories to be more properly unraveled. The cooling rate plays an important role in the eventual degassing pattern seen in shocked ordinary chondrite material. A more detailed comparison of the cooling rates of L and H chondrites with their Ar degassing patterns may shed more light on the likelihood of a meteorite retaining excess Ar and the constraints that can be placed on the ages of thermal impacts.

Orvinio and other H chondrites show evidence of having been subjected to multiple impact degassing events. Orvinio's CRE age of 7.5 Ma and possible upper Ar plateau age of ~4.2 Ga indicate that it could have been involved in H chondrite events of 7–8 Ma and ~4.3 Ga, as suggested by previous studies. Additionally, Orvinio clearly has been involved in at least one other impact event in the last 600 Ma, perhaps in the last 325 Ma. A complex impact history is required to create meteorites with the same CRE ages that have different Ar degassing histories. This implies a somewhat heterogeneous surface for the H chondrite parent body.

Shock darkening of meteorites can be quantified with opaque counts. Opaque counts conducted on both the melt and clast fractions of a shocked meteorite illustrate the mechanisms that produce darkening and the different levels achieved between separate phases (Britt 1991). The shock metamorphism that redistributed the opaque minerals lowers the overall albedo of the meteorite and subdues the absorption features, producing characteristic reflectance spectra. Although this is a result of the same shock that led to Ar degassing, the opaque redistribution probably occurred in the first fraction of a second, at much higher temperatures than those that outgassed Ar. Ironically, the material that was most affected texturally by the shock, the melt, is not as strongly affected spectrally (because it was heated enough that opaques could recoalesce), nor is it as degassed (because it ended up with diffusion properties less susceptible to degassing during the later, slower cooling). Our analyses of the spectra from Orvinio and comparisons with other meteorites and asteroids indicate that remote sensing of an asteroid dominated by Orvinio-like material would not lead to an interpretation of such an object being made of OC material, given visible-only data. If the remote spectra were extended into the infrared, it would be difficult to identify what type of OC meteorite was the parent body. The existence of relatively small amounts of Orvinio-like material on an asteroid may skew its spectrum away from laboratory-based OC spectra and complicate its identification. However, the fact that shock metamorphism lowers the albedo of an object without increasing its spectral slope may partially explain the spectral trends seen on 433 Eros by the NEAR Shoemaker spacecraft.

Acknowledgments–We greatly appreciate constructive reviews of this manuscript and an earlier version by B. Clark, D. Bogard, and two anonymous reviewers, and we thank R. Wieler for his work as Associate Editor. We thank Dr. Guy Consolmagno of the Vatican for providing the samples we used. This work was supported primarily by NASA grants NAG 5–12059 (T. Swindle) and NAG 5–12881 (D. Kring).

Editorial Handling—Dr. Rainer Wieler

REFERENCES

Alexeev V. A. 1995. Catastrophe in space: 500 or 300 Myr ago? 26th Lunar and Planetary Science Conference. pp. 19–20.

Alexeev V. A. 1998. Parent bodies of L and H chondrites: Times of catastrophic events. *Meteoritics & Planetary Science* 33:145–152.

Bogard D. D. 1995. Impact ages of meteorites: A synthesis. *Meteoritics* 30:244–268.

Bogard D. D. and Garrison D. H. 1999. ^{39}Ar-^{40}Ar dating of thermal events on meteorite parent bodies (abstract #1104). 30th Lunar and Planetary Science Conference. CD-ROM.

Bogard D. D., Garrison D. H., and Masarik J. 2001. The Monahans chondrite and halite: Argon-39/argon-40 age, solar gases, cosmic ray exposure ages, and parent body regolith neutron flux and thickness. *Meteoritics & Planetary Science* 36:107–122.

Bogard D. D., Garrison D. H., Norman M., Scott E. R. D., and Keil K. 1995. $^{39}Ar/^{40}Ar$ age and petrology of Chico: Large-scale melting on the L chondrite parent body. *Geochimica et Cosmochimica Acta* 59:1383–1399.

Bogard D. D. and Hirsch W. C. 1980. $^{40}Ar/^{39}Ar$ dating, Ar diffusion properties, and cooling rate determinations of severely shocked chondrites. *Geochimica et Cosmochimica Acta* 44:1667–1682.

Bogard D. D., Husain L., and Wright R. J. 1976. ^{40}Ar-^{39}Ar dating of collisional events in chondrite parent bodies. *Journal of Geophysical Research* 81:5664–5678.

Britt D. T. 1991. The meteorite record as clues to asteroid regolith processes. PhD thesis, Brown University, Providence, Rhode Island.

Britt D. T. and Pieters C. M. 1991. Black ordinary chondrites: An analysis of abundance and fall frequency. *Meteoritics* 26:279–285.

Britt D. T. and Pieters C. M. 1994. Darkening in black and gas-rich ordinary chondrites: The spectral effects of opaque morphology and distribution. *Geochimica et Cosmochimica Acta* 58:3905–3919.

Bus S. J. and Binzel R. P. 2002. Phase II of the Small Main-belt

Asteroid Spectroscopic Survey—A feature-based taxonomy. *Icarus* 158:146–177.

Clark B. E., Helfenstein P., Bell J. F., Peterson C., Veverka J., Izenberg N. I., Dominique D., Wellnitz D., and McFadden L. 2002. NEAR infrared spectrometer photometry of asteroid 433 Eros. *Icarus* 155:189–204.

Clark R. N. 1983. Spectral properties of mixtures of montmorillonite and dark grains: Implications for remote sensing. *Journal of Geophysical Research* 88:10635–10644.

Deutsch A. and Scharer U. 1994. Dating terrestrial impact events. *Meteoritics* 29:301–302.

Eugster O. 1988. Cosmic ray production rates for ^{3}He, ^{21}Ne, ^{38}Ar, ^{83}Kr, and ^{126}Xe in chondrites based on ^{81}Kr-Kr exposure ages. *Geochimica et Cosmochimica Acta* 52:1649–1662.

Foland K. A. 1974. ^{40}Ar diffusion in homogeneous orthoclase and interpretation of argon diffusion in K-feldspars. *Geochimica et Cosmochimica Acta* 38:151–166.

Folco L., Bland P. A., D'Orazio M., Franchi I. A., Kelley S. P., and Rocchi S. 2004. Extensive impact melting on the H chondrite parent asteroid during the cataclysmic bombardment of the early solar system: Evidence from the achondritic meteorite Dar al Gani 896. *Geochimica et Cosmochimica Acta* 68:2379–2397.

Gaffey M. J. 1976. Spectral reflectance characteristics of the meteorite classes. *Journal of Geophysical Research* 81:905–920.

Gaffey M. J., Bell J. F., Brown R. H., Burbine T. H., Piatek J. L., Reed K. L. and Chaky D. A. 1993. Mineralogical variations within the S-type asteroid class. *Icarus* 106:573–602.

Gaffey M. J., Bell J. F., and Cruikshank D. P. 1989. Reflectance spectroscopy and asteroid surface mineralogy. In *Asteroids II,* edited by Binzel R. P., Gehrels T., and Matthews M. S., Tucson: University of Arizona Press. pp. 98–127.

Gaffey M. J. and Gilbert S. L. 1998. Asteroid 6 Hebe: The probable parent body of the H-type ordinary chondrites and the IIE iron meteorites. *Meteoritics & Planetary Science* 33:1281–1295.

Garrison D., Hamlin S., and Bogard D. 2000. Chlorine abundances in meteorites. *Meteoritics & Planetary Science* 35:419–429.

Grady M. M. 2000. *Catalogue of meteorites: With special reference to those represented in the collection of the Natural History Museum, London, 5th edition.* New York: Cambridge University Press. 689 p.

Graf T. and Marti K. 1995. Collisional history of H chondrites. *Journal of Geophysical Research* 100:21247–21263.

Grier J. A., Swindle T. D., and Kring D. A. 1996. The impact evolution of L chondrite parent body material. *Meteoritics & Planetary Science* 31:A55.

Haack H., Farinella P., Keil K., and Scott E. R. D. 1996. Meteoritic, asteroidal, and theoretical constraints on the 500 Ma disruption of the L chondrite parent body. *Icarus* 119:182–191.

Heymann D. 1967. On the origin of hypersthene chondrites: Ages and shock effects of black chondrites. *Icarus* 6:189–221.

Jessberger E. K., Kirsten T., and Staudacher T. 1976. Argon-argon ages of consortium breccia 73215. Proceedings, 7th Lunar and Planetary Science Conference. pp. 2201–2215.

Kring D. A., Swindle T. D., Britt D. T., and Grier J. A. 1996. Cat Mountain: A meteoritic sample of an impact-melted asteroid regolith. *Journal of Geophysical Research* 101:29353–29371.

Kring D. A., Swindle T. D., Cohen B. A., and Hill D. H. 2000. Regolith breccia (Ourique) with impact melt clasts and other debris from an H chondrite parent body (abstract #1688). 31st Lunar and Planetary Science Conference. CD-ROM.

Kunz J., Falta M., and Jessberger E. K. 1997. Shocked meteorites: Argon-40-argon-39 evidence for multiple impacts. *Meteoritics & Planetary Science* 32:647–670.

Lanphere M. A. and Dalrymple G. B. 1976. Identification of excess ^{40}Ar by the ^{40}Ar/^{39}Ar age spectrum technique. *Earth and Planetary Science Letters* 32:141–148.

Mason B. 1963. Olivine composition in chondrites. *Geochimica et Cosmochimica Acta* 27:1011–1023.

McConville P. S., Kelley S., and Turner G. 1988. Laser probe ^{40}Ar-^{39}Ar studies of the Peace River shocked L6 chondrite. *Geochimica et Cosmochimica Acta* 52:2487–2499.

McDougall I. and Harrison T. M. 1999. *Geochronology and thermochronology by the ^{40}Ar/^{39}Ar method.* New York: Oxford University Press. 269 p.

Nittler L. R., Starr R. D., Lim L., McCoy T. J., Burbine T. H., Reedy R. C., Trombka J. I., Gorenstein P., Squyres S. W., Boynton W. V., McClanahan T. P., Bhangoo J. S., Clark P. E., Murphy M. E., and Killen R. 2001. X-ray flourescence measurements of the surface elemental composition of asteroid 433 Eros. *Meteoritics & Planetary Science* 36:167–1695.

Noble S. K., Pieters C. M., Taylor L. A., Morris R. V., Allen C. C., McKay D. S., and Keller L. P. 2001. The optical properties of the finest fraction of lunar soil: Implications for space weathering. *Meteoritics & Planetary Science* 36:31–42.

Pieters C. M. 1983. Strength of mineral absorption features in the transmitted component of near infrared reflected light: First results from RELAB. *Journal of Geophysical Research* 88:9534–9544.

Pieters C. M., Taylor L. A., Noble S. K., Keller L. P., Hapke B. W., Morris R. V., Allen C. C., McKay D. S., and Wentworth S. 2000. Space weathering on airless bodies: Resolving a mystery with lunar samples. *Meteoritics & Planetary Science* 35:1101–1107.

Rock-Color Chart Committee 1991. *The rock color chart.* Boulder: Geological Society of America.

Salpeter E. W. 1957. *The Vatican collection of meteorites.* Citta del Vaticana: Specola Vaticana.

Salvatori R., Maras A., and King E. A. 1986. *The Vatican collection of meteorites.* Citta del Vaticana: Specola Vaticana.

Schmitz B., Häggström T., and Tassinari M. 2003. Sediment-dispersed extraterrestrial chromite traces major asteroid disruption event. *Science* 300:961–964.

Schultz L. and Kruse H. 1989. Helium, neon, and argon in meteorites—A data compilation. *Meteoritics* 24:155–172.

Scott E. R. D., Maggiore P., Taylor G. J., Keil K., and Szuwalski D. 1986. Chondritic impact melts and cratering processes on asteroids. 17th Lunar and Planetary Science Conference. pp. 785–786.

Scott E. R. D., Taylor G. J., Newsom H. E., Herbert F., Zolensky M., and Kerridge J. F. 1989. Chemical, thermal, and impact processing of asteroids. In *Asteroids II,* edited by Binzel R. P., Gehrels T., and Matthews M. S. Tucson: University of Arizona Press.

Sears D. W. G. and Dodd R. T. 1988. Overview and classification of meteorites. In *Meteorites and the early solar system,* edited by Kerridge J. F. and Matthews M. S. Tucson: University of Arizona Press. pp. 3–31.

Smith B. A. and Goldstein J. I. 1977. The metallic microstructures and thermal histories of severely reheated chondrites. *Geochimica et Cosmochimica Acta* 41:1061–1072.

Stöffler D., Keil K., and Scott E. R. D. 1991. Shock metamorphism of ordinary chondrites. *Geochimica et Cosmochimica Acta* 55: 3845–3867.

Trieloff M., Reimold W. U., Kunz J., Boer R. H., and Jessberger E. K. 1994. ^{40}Ar-^{39}Ar thermochronology of pseudotachylite at the Ventersdorp contact reef, Witwatersrand basin. *South African Journal of Geology* 97:365–384.

Wasson J. T. and Wang S. 1991. The histories of ordinary chondrite parent bodies: U, Th-He age distributions. *Meteoritics* 26:161–167.

APPENDIX

Table A1. Argon in Orvinio clast sample OCA1 (22.7 mg). The apparent ages are shown with the total error (includes error due to uncertainty in J factor).

Temp (C)	^{39}Ar ccSTP/gm $\times 10^{-10}$	^{36}Ar/^{39}Ar	^{37}Ar/^{39}Ar	^{38}Ar/^{39}Ar	^{40}Ar/^{39}Ar	Appar. age (Ma)
400	1.58	66.6	3.5	12.5	26000	6400
		3.6	1.0	0.7	1400	100
450	1.98	3.27	3.2	0.867	1232	17178
		0.14	0.7	0.040	46	44
500	2.38	1.24	2.2	0.502	587	1019
		0.06	0.6	0.031	25	34
550	2.77	1.50	2.2	0.596	753	1226
		0.05	0.7	0.030	20	26
600	4.03	0.684	2.97	0.523	526	936
		0.028	0.45	0.015	11	18
631	2.33	0.659	3.2	0.610	475	864
		0.036	0.7	0.025	15	24
650	4.30	0.324	2.46	0.471	288	570
		0.020	0.47	0.017	6	12
675	2.03	0.475	3.2	0.498	443	817
		0.037	0.8	0.023	14	24
700	1.45	0.47	4.7	0.598	520	927
		0.05	1.1	0.040	23	34
750	2.16	0.349	2.8	0.579	503	9023
		0.042	0.6	0.025	20	30
825	3.16	0.483	2.6	0.790	535	948
		0.036	0.6	0.034	16	25
925	3.37	1.146	4.7	1.352	794	1273
		0.039	0.5	0.048	17	23
1025	6.09	1.339	6.68	1.162	1802	2169
		0.029	0.36	0.027	278	26
1075	5.55	1.76	12.4	1.214	3330	3011
		0.06	1.3	0.044	110	51
1100	4.45	2.07	11.6	1.061	3890	3240
		0.06	0.6	0.026	84	38
1110	3.06	1.98	10.0	1.16	4090	3317
		0.09	1.0	0.05	160	61
1150	3.64	2.90	11.0	1.27	5000	3620
		0.11	0.8	0.05	170	60
1200	4.03	3.86	10.7	1.432	4860	3580
		0.10	0.7	0.040	130	40
1250	4.07	4.41	9.3	1.503	4479	3455
		0.10	0.5	0.034	73	32
1300	2.75	6.02	10.1	1.94	5100	3656
		0.27	1.1	0.09	220	70
1400	3.09	7.47	10.6	2.23	5460	3763
		0.30	0.9	0.10	210	64
Total	68.29	3.65	6.88	1.331	3000	2858
		0.12	0.18	0.023	50	27

Table A2. Argon in Orvinio clast sample OCA2 (26.0 mg). The apparent ages are shown with the total error (includes error due to uncertainty in J factor). Note that the 1125° step is not represented in the argon spectrum for OCA2. It is listed here for completeness, but as an experimental error occurred during gas extraction during this step, the age is not meaningful. Therefore, it has been left out of the argon spectrum.

Temp (C)	^{39}Ar ccSTP/gm $\times 10^{-10}$	^{36}Ar/^{39}Ar	^{38}Ar/^{39}Ar	^{40}Ar/^{39}Ar	Appar. age (Ma)
400	5.22	11.1	2.49	3860	3230
		1.0	0.24	330	130
500	2.69	1.433	0.610	1126	1620
		0.040	0.022	20	24
550	5.83	0.276	0.336	152.4	324
		0.012	0.011	2.0	6
600	6.51	0.436	0.461	270.5	541
		0.018	0.009	2.7	8
630	4.44	0.529	0.531	353	678
		0.018	0.015	7	13
660	2.60	0.311	0.528	354	680
		0.026	0.019	11	19
690	2.51	0.848	0.735	541	956
		0.044	0.037	16	24
720	1.65	0.522	0.756	693	1154
		0.042	0.031	21	28
750	1.54	0.728	0.87	859	1346
		0.048	0.040	24	29
780	1.25	0.89	1.10	1229	1715
		0.07	0.07	42	41
820	1.62	1.79	1.98	1837	2194
		0.06	0.06	43	35
875	2.23	1.31	1.335	2385	2537
		0.05	0.038	44	31
925	2.08	1.75	1.402	2790	2757
		0.06	0.050	80	44
980	2.71	1.335	1.083	2990	2855
		0.045	0.034	60	33
1025	3.87	1.13	0.76	2920	2820
		0.16	0.10	320	160
1075	4.29	1.12	0.79	3440	3060
		0.14	0.11	280	120
1100	3.80	1.26	0.68	3610	3130
		0.15	0.09	320	130
1125	6.81	0.92	0.369	1220	1710
		0.09	0.043	90	90
1150	1.36	2.88	1.34	5060	3640
		0.14	0.08	250	8
1200	2.92	3.0	1.35	5300	370
		0.5	0.30	900	290
1250	4.33	3.46	1.40	4140	3330
		0.36	0.18	420	160
1300	4.19	5.8	1.67	4820	3570
		0.5	0.20	440	140
1400	5.75	5.00	1.70	510	3660
		0.44	0.19	420	130
Total	80.18	2.36	1.011	2410	2680
		0.09	0.030	70	30

Table A3. Argon in Orvinio clast sample OCA3 (20.4 mg). The apparent ages are shown with the total error (includes error due to uncertainty in J factor).

Temp (C)	^{39}Ar ccSTP/gm $\times 10^{-10}$	^{36}Ar/^{39}Ar	^{38}Ar/^{39}Ar	^{40}Ar/^{39}Ar	Appar. age (Ma)
500	6.34	6.8	1.73	2780	2750
		0.8	0.22	340	170
520	1.35	1.92	0.757	1237	1723
		0.09	0.047	49	47
540	2.32	0.621	0.364	455	835
		0.049	0.028	15	24
560	5.21	0.437	0.407	373	711
		0.015	0.016	7	14
580	2.68	0.566	0.436	385	729
		0.034	0.017	9	16
590	3.98	0.507	0.456	368	703
		0.026	0.023	7	14
600	1.78	0.64	0.488	480	871
		0.05	0.024	13	21
625	1.66	0.80	0.585	555	977
		0.06	0.034	18	27
650	1.82	0.65	0.570	601	1038
		0.06	0.040	27	37
675	1.70	0.87	0.61	675	1132
		0.06	0.05	33	43
700	1.47	1.11	0.78	1032	1529
		0.07	0.08	45	48
725	1.68	1.14	0.688	1040	1540
		0.10	0.048	60	70
750	1.38	1.25	0.82	1093	1588
		0.07	0.05	39	41
800	1.92	2.02	1.30	1337	1810
		0.09	0.06	44	41
850	1.73	1.86	1.07	1680	2080
		0.10	0.06	80	60
900	1.59	2.42	1.06	205	2334
		0.09	0.07	6	44
950	2.61	3.25	1.34	2260	2460
		0.14	0.06	80	50
1000	3.31	3.01	1.250	3000	2857
		0.06	0.032	60	34
1050	5.24	3.66	1.357	3690	3160
		0.06	0.028	60	31
1075	2.65	3.12	1.22	3830	3220
		0.11	0.06	120	50
1100	2.73	3.19	1.221	3580	2076
		0.10	0.041	110	29
1125	3.91	3.51	1.25	4120	3120
		0.11	0.07	130	50
1150	4.98	4.07	1.77	4840	3328
		0.53	0.24	640	50
1200	6.11	5.0	1.62	4020	3560
		0.5	0.19	450	210
1250	2.82	8.64	2.412	4930	3290
		0.29	0.12	160	170
1300	2.21	11.7	2.82	5307	3600
		0.5	0.13	230	60
1400	6.43	16.7	4.1	5200	3720
		2.3	0.6	700	70
Total	81.59	4.30	1.42	2710	2713
		0.21	0.06	90	39

Table A4. Argon in Orvinio melt sample OMA5 (6.59 mg). The apparent ages are shown with the total error (includes error due to uncertainty in J factor).

Temp (C)	^{39}Ar ccSTP/gm $\times 10^{-10}$	^{36}Ar/^{39}Ar	^{37}Ar/^{39}Ar	^{38}Ar/^{39}Ar	^{40}Ar/^{39}Ar	Appar. age (Ma)
400	1.00	140	6	27	58000	7800
		38	6	7	16000	500
500	2.47	4.6	2.6	1.35	3620	3130
		0.5	2.3	0.16	40	170
550	2.25	1.48	–1.0	0.79	1130	1620
		0.18	2.7	0.11	120	110
600	1.90	0.59	4.7	0.75	890	1380
		0.15	3.2	0.09	80	90
700	2.99	0.56	3.5	0.80	980	1480
		0.09	2.1	0.09	70	70
775	5.66	0.37	1.1	0.506	500	904
		0.05	0.9	0.037	20	30
850	4.28	0.56	1.9	0.77	1110	1600
		0.09	1.4	0.06	60	60
900	2.57	0.30	–0.3	0.70	990	1490
		0.16	2.7	0.05	60	70
950	1.87	0.32	2.1	0.82	1590	2020
		0.22	3.2	0.11	150	110
1000	2.96	0.55	6.5	0.67	1970	2280
		0.16	2.5	0.07	190	130
1050	1.72	1.26	19.4	1.31	3700	3170
		0.29	4.7	0.20	600	220
1100	2.03	1.57	15.8	1.18	6500	4050
		0.28	4.1	0.12	600	160
1150	1.94	1.90	9.6	1.27	7400	4250
		0.31	3.5	0.15	800	190
1200	3.22	1.94	12.6	1.25	7000	4170
		0.24	2.9	0.11	600	130
1250	2.90	3.12	10.5	1.57	7100	4180
		0.34	2.7	0.15	700	160
1300	6.99	3.12	12.4	1.35	7860	4350
		0.16	1.7	0.05	230	50
1325	10.31	3.13	9.4	1.259	7740	4325
		0.11	0.9	0.036	160	40
1350	10.71	3.42	8.0	1.32	8110	4400
		0.15	0.9	0.05	280	60
1375	1.74	13.6	8.5	3.6	12100	5070
		1.9	4.3	0.5	1700	250
1400	0.08	120	30	30	40000	7200
		360	140	80	120000	4800
Total	69.69	4.5	7.3	1.56	5980	3908
		0.7	0.5	0.15	290	36

Table A5. Argon in Orvinio melt sample OMA6 (30.9 mg). The apparent ages are shown with the total error (includes error due to uncertainty in J factor).

Temp (C)	^{39}Ar ccSTP/gm $\times 10^{-10}$	^{36}Ar/^{39}Ar	^{38}Ar/^{39}Ar	^{40}Ar/^{39}Ar	Appar. age (Ma)
425	0.273	6.5	1.84	4100	3330
		1.3	0.38	800	320
500	1.116	2.89	1.05	2830	2770
		0.19	0.07	180	90
550	1.638	1.240	0.695	1454	1908
		0.047	0.030	46	40
600	1.801	0.750	0.68	876	1366
		0.039	0.05	29	34
650	2.130	0.435	0.592	523	932
		0.028	0.023	13	20
700	2.572	0.333	0.591	519	926
		0.023	0.016	11	18
750	2.400	0.261	0.541	516	922
		0.027	0.021	12	20
800	2.117	0.398	0.540	768	1243
		0.034	0.019	19	26
850	2.342	0.303	0.551	719	1185
		0.034	0.020	21	28
900	1.519	0.71	1.36	1159	1651
		0.06	0.05	41	41
950	1.425	0.65	1.08	1490	1940
		0.07	0.05	60	50
1025	2.083	0.90	0.963	2330	2503
		0.06	0.045	70	47
1100	2.125	1.28	1.12	3710	3170
		0.07	0.06	150	60
1250	5.323	4.92	2.57	6770	4110
		0.20	0.15	280	70
1325	15.504	4.92	2.367	7130	4190
		0.12	0.016	200	50
1350	2.299	3.40	1.314	8060	4390
		0.14	0.050	280	60
1375	0.375	13.5	3.57	12000	5060
		1.9	0.52	1700	240
1400	0.019	120	30	40000	7100
		340	70	110000	4800
Total	47.060	2.90	1.568	4300	3391
		0.15	0.039	100	34

Table A6. Argon in Orvinio melt sample OMA7 (33.4 mg). The apparent ages are shown with the total error (includes error due to uncertainty in J factor).

Temp (C)	^{39}Ar ccSTP/gm $\times 10^{-10}$	^{36}Ar/^{39}Ar	^{38}Ar/^{39}Ar	^{40}Ar/^{39}Ar	Appar. age (Ma)
380	0.0155	128	23	78000	8330
		28	5	17000	410
435	0.1599	1.49	0.755	814	1296
		0.09	0.036	21	27
475	0.1522	0.94	0.700	584	1014
		0.10	0.047	24	33
500	0.1879	0.62	0.653	468	854
		0.10	0.036	16	25
525	0.1703	0.42	0.510	390	735
		0.11	0.046	18	29
550	0.1544	0.32	0.68	338	654
		0.12	0.05	22	36
575	0.1492	0.42	0.655	279	555
		0.13	0.047	23	40
600	0.2610	0.38	0.615	262	526
		0.07	0.046	14	25
625	0.2524	0.31	0.615	392	738
		0.07	0.034	14	22
650	0.2790	0.21	0.600	268	536
		0.07	0.030	12	21
675	0.3107	0.21	0.531	276	550
		0.06	0.031	10	18
700	0.2925	0.23	0.573	297	586
		0.06	0.039	13	23
725	0.2623	0.29	0.641	403	756
		0.06	0.033	15	25
750	0.2504	0.30	0.692	442	815
		0.07	0.040	15	24
775	0.2364	0.33	0.71	573	999
		0.07	0.03	16	24
800	0.1704	0.54	0.87	764	1239
		0.10	0.06	36	43
850	0.1809	1.27	1.70	1128	1622
		0.10	0.08	37	38
900	0.1962	1.32	1.222	1683	2084
		0.06	0.045	27	26
950	0.0964	1.65	1.14	2770	2742
		0.13	0.08	80	43
1050	0.1745	2.18	1.65	4050	3300
		0.16	0.07	130	50
1200	0.1422	5.72	2.50	6480	4038
		0.24	0.09	180	50
1400	0.0451	0.1	0.62	6400	4010
		1.3	0.38	600	140
1515	0.0014	340	60	90000	8500
		310	50	70000	2100
Total	4.1412	1.37	0.939	1305	1783
		0.15	0.029	70	26